A Highly-Accurate Robot Calibration Method with Line Constraint

Tinghui Chen
School of Computer Science and Technology
Chongqing University of Posts and Telecommunications,
Chongqing, China
chenth199208@outlook.com

Shuai Li
Faculty of Information Technology and Electrical Engineering
University of Oulu
Technology Research Center of Finland (VTT)
Oulu, Finland
shuai.li@oulu.fi

Xin Luo
College of Computer and Information Science
Southwest University
Chongqing, China
luoxin@swu.edu.cn

***Abstract*—For the application of industrial robots, positioning accuracy is a significant indicator of their performance. Aiming at the issues of low positioning accuracy, the calibration techniques are employed to obtain the real kinematic parameters for effectively enhancing its accuracy. However, in practical scenarios, for the restriction of the robot workspace, the samples collected during the robot calibration process cannot cover the entire space of the entire space, resulting in an impact on data integrity. To address the above issues, we develop a calibrator integrating the MCS method (measurement configurations selection) and LM algorithm (Levenberg-Marquardt) with a spatial line constraint (LMLC), which contains three-fold: a) selecting a set of most representative measurement configurations according to the observability index for enhancing the stability of calibration results; b) develop an LM algorithm with line constraint to solve the problem of spatial restriction of robot sampling; c) presenting a robot calibrator that combines MCS and LMLC for efficiently improving the robot calibration accuracy. Experiments illustrate that the MCS-LMLC calibrator outperforms state-of-the-art calibrators on an industrial robot's calibration accuracy and computational efficiency.**

***Keywords*—Robot calibration, positioning error, measurement configurations selection, observability index, Levenberg-Marquardt algorithm, calibrator.**

I. INTRODUCTION

Nowadays, the industrial robot is a great integration of industrialization and informatization, which can be regarded as a crucial indicator of a country's innovation capability and industrial competitiveness [1]-[3]. However, due to factors like machining, assembly, etc., robots' absolute positioning accuracy is far lower than many application requirements, e.g., the precision grinding of complex surfaces [4]-[9]. Therefore, enhancing the absolute positioning accuracy has become a focal issue for robot researchers. Moreover, the most significant factors of the positioning errors affecting accuracy are divided into geometric errors and non-geometric errors, among which geometric factors mainly contain assembly errors, manufacturing errors, wear, etc., accounting for 90% of the total error [9]-[13]. Hence, we only take into account the geometric errors as the research objectives to achieve kinematic parameters calibration.

Traditionally, for the kinematic parameters calibration techniques, enough samples that cover the entire space of the robot are prerequisites to ensure data completeness and correctness of calibration results [14]-[20]. However, in real environments, the robot workspace is frequently constricted, resulting in incomplete data collection. To address this issue, researchers have developed many spatial constraint calibration techniques. Lembono *et al*. [6] adopt a laser and a tooltip to constrain a robot calibration space with planes and distances, achieving a maximum error reduction from 1.41 to 0.5 mm. Stepanova *et al*. [7] combine self-contact, plane constraint and self-observation methods for robot calibration and verified their performance in terms of calibration accuracy. He *et al*. propose [12] a robot calibration method utilizing multiple position constraints for enhancing an industrial robot's accuracy. The method calibrates the kinematic parameters of the robot by controlling it to reach the same position in different postures, which can achieve high accuracy and rapid convergence of the robot. Based on the above analyses, we propose a robot accuracy calibrator incorporating a spatial line constraint into Levenberg-Marquardt (LM) algorithm to achieve robot calibration in constrained space [21]-[27].

In addition, considering that different end measurement configuration sets under the same error model can bring different kinematic parameter identification results [14]-[18]. Therefore, selecting a set of optimal measurement configurations before calibration is instrumental in enhancing the stability of experimental results. Jiang *et al*. [13] obtain better measurement poses according to the observability index results, achieving accuracy improvement. Fu *et al*. [18] employ an observability index to optimize calibration poses, eliminating torque error constraints. Wang *et al*. [14] propose an improved particle swarm optimization method and employ it for optimal measurement selection. The results illustrate the feasibility and advantages of the method. Hence, this paper employs the SA algorithm (simulated annealing) to obtain the optimal measurement configurations of the calibration configurations.

The main contributions of this work include:

a) Selecting the optimal number and set of pose points based on the observability index, which can effectively enhance unstable calibration results;

b) Proposing an LM algorithm with a spatial linear constraint (LMLC), which addresses the issue of measurement space restriction;

c) Presenting the MCS-LMLC calibrator, which can effectively decrease measurement noises for enhancing the stability of experimental results.

TABLE I. THE D-H PARAMETERS OF AN HRS JR680 ROBOT.

Joint *i*	α_i/°	a_i/*mm*	d_i/*mm*	θ_i/°
1	-90.00	250.00	653.50	0.00
2	0.00	900.00	0.00	-90.00
3	-90.00	-205.00	0.00	180.00
4	90.00	0.00	1030.20	0.00
5	-90.00	0.00	0.0	90.00
6	0.00	0.00	200.60	0.00

I. PRELIMINARIES

This work adopts the D-H model to establish the forward kinematics model of an industrial robot [28]-[30], whose kinematics expression between adjacent links can be given as:

$$A_i = \begin{bmatrix} c\theta_i & -s\theta_i c\alpha_i & s\theta_i s\alpha_i & a_i c\theta_i \\ s\theta_i & c\theta_i c\alpha_i & -c\theta_i s\alpha_i & a_i s\theta_i \\ 0 & s\alpha_i & c\alpha_i & d_i \\ 0 & 0 & 0 & 1 \end{bmatrix}, \tag{1}$$

where θ_i, α_i, a_i, d_i represent a joint angle, a link twist angle, a link length and a link offset, respectively. Table I shows the initial values of them.

Note that the nominal pose matrix T_w in D-H model can be expressed as:

$$T_w = A_1A_2A_3A_4A_5A_6 = \begin{bmatrix} n_x & o_x & c_x & P_x \\ n_y & o_y & c_y & P_y \\ n_z & o_z & c_z & P_z \\ 0 & 0 & 0 & 1 \end{bmatrix} = \begin{bmatrix} R_w & P_w \\ 0 & 1 \end{bmatrix}, \tag{2}$$

where R_w and P_w refer to the nominal pose matrix and position vector, respectively. With an error in the kinematic parameters, the corresponding actual pose matrix is T_r, and the pose error matrix ΔT is famulated as:

$$\Delta T = T_r - T_w = \begin{bmatrix} \Delta R & \Delta p \\ 0 & 1 \end{bmatrix}, \tag{3}$$

where $\Delta R=[\Delta n, \Delta o, \Delta c]$ is the pose error at an industrial robot's end-effector, Δp refers to the positional error at the end.

Then, the kinematic errors model can be expressed as:

$$\Delta E = J\Delta X, \tag{4}$$

where $\Delta E=[\Delta n^T, \Delta o^T, \Delta c^T, \Delta p^T]^T$ is the kinematic errors matrix, $J=[\Delta n^T, \Delta o^T, \Delta c^T, \Delta p^T]^T$ is the Jacobian matrix of the kinematic errors matrix, $\Delta X=[\Delta\theta, \Delta a, \Delta\alpha, \Delta d]^T$ refers to the error of robot kinematic parameters.

II. KINEMATIC PARAMETER IDENTIFICATION

A. Measurement Configurations Selection (MCS)

The calibration accuracy and experiment stability depend on the number and spatial distribution of calibration configurations [13]. To measure the quality of the measurement configurations set, observability indices are employed to evaluate it. Furthermore, according to the Jacobian matrix J's singular values, Δx is observable when J^TJ is full rank. The commonly used observability indices are O_1, O_2, O_3, O_4, O_5, which is formulated as [14]-[18]:

$$\begin{aligned} &O_1 = \frac{\sqrt{\sigma_1\sigma_1\cdots\sigma_m}}{\sqrt{N_0}}, O_2 = \frac{\sigma_m}{\sigma_1}, O_3 = \sigma_m, \\ &O_4 = \frac{\sigma_m^2}{\sigma_1}, O_5 = \frac{1}{\sigma_1} + \frac{1}{\sigma_2} + \cdots + \frac{1}{\sigma_m}, \end{aligned} \tag{5}$$

where m refers to the number of singular values (σ_1, σ_2, ⋯, σ_m), N_0 is the number of measurement configurations.

In the process of measurement configurations selection, the first step is to define the appropriate number of it. Generally, as the number of measurement configurations increases, the observability indices will gradually stabilize, which corresponds to the number of optimal measurement configurations, denoted by N. Then, a simulated annealing algorithm is employed to select N optimal measurement configurations in N_0 measurement configurations.

B. LMLC Algorithm

The critical issue in establishing the minimization objective model is the introduction of spatial constraints. Hence, this paper defines the spatial line constraint equation as:

$$\frac{\hat{x}-x'}{l_{\hat{x}}} = \frac{\hat{y}-y'}{l_{\hat{y}}} = \frac{\hat{z}-z'}{l_{\hat{z}}}, \tag{6}$$

Then, the spatial line constraint of this work can be further depicted as:

$$\begin{aligned} &\Phi_{i,M}\left(\hat{w}, \hat{P}, \beta'\right) = \left[f_i\left(\hat{w}\right) - \hat{P} \right]^T \beta' M = 0, \\ &\Phi_{i,K}\left(\hat{w}, \hat{P}, \beta'\right) = \left[f_i\left(\hat{w}\right) - \hat{P} \right]^T \beta' K = 0, \end{aligned} \tag{7}$$

where $\Phi_{i,M}$ and $\Phi_{i,K}$ represent the constraint equation of the spatial line, $\hat{w}$ is the D-H parameters, $\hat{P}$ refers to a point of the spatial line, β' represents the direction vector of a spatial line, $f_i(w)$ refers to a nominal point of the spatial line, M and K can be given as:

$$M = \begin{bmatrix} 1 & 0 & 0 \\ 0 & 0 & 0 \\ 0 & 0 & -1 \end{bmatrix}, K = \begin{bmatrix} 0 & 0 & 0 \\ 0 & 1 & 0 \\ 0 & 0 & -1 \end{bmatrix} \tag{8}$$

Based on the LM algorithms' principle, we incorporate the spatial line constraint into the LM algorithm to establish the objective function as:

$$\begin{aligned} L &= \arg\min_{w} \left\| Y_i - F_i\left(\hat{w}\right) \right\|_2^2 \\ &= \frac{1}{2N}\sum_{i=1}^{N} \left\| Y_i - F_i\left(\hat{w}_t, P_{0,t}\right) - \nabla_w F_i\left(\hat{w}_{t+1} - \hat{w}_t\right) - \nabla_{P_{0,t}} F_i\left(P_{0,t+1} - P_{0,t}\right) \right\|_2^2 \\ &\quad + \frac{\lambda}{2}\left[\left(\hat{w}_{t+1} - \hat{w}_t\right)^2 + \left(P_{0,t+1} - P_{0,t}\right)^2 \right], \\ &s.t. \left[f_i\left(\hat{w}\right) - \hat{P} \right]^T \beta' M = 0; \left[f_i\left(\hat{w}\right) - \hat{P} \right]^T \beta' K = 0, \end{aligned} \tag{9}$$

where $F(\hat{w}, P_0)$ represents the distance between the fixed point coordinate of the drawstring displacement sensor on the ground (P_0) and a robot's end-effector. Y refers to the cable-measured length of the drawstring, λ is the regularization coefficient. Note that, p is a preprocessed value. Then, (9) can be further famulated as:

Algorithm I: MCS-LMLC

Input: w_0, I_1, I_2, I_3, N_0, $\{q_{i,1}, q_{i,2}, \ldots, q_{i,6}\}$, $\{Y_1, Y_2, \ldots, Y_{N0}\}$, β_0, p_0, P_0, λ

Operation

/* Initialization */

Initialize m, ρ_r, $w=w_0$, $p=p_0$, $P=P_0$, $\beta=\beta_0$,

/* Training-MCS Step*/

for $t=m$ to N_0
  Calculate the observability indexes via (5)
end for
Based on the results of the observability indexes to output N
for k_1=1 to I_1
  Generate N configurations from N_0 configurations
  Calculate the observability indexes via (5)
  Achieving the MCS according to the SA algorithm
end for

Output N measurement configurations

/* Training-AMPC Step */

Input N measurement configurations

for k_2=1 to I_2
  for i=1 to N
    Updating the β_{t+1} and P_{t+1} based on (11) and (12).
  end for
end for
Output β_{t+1} and P_{t+1}
for k_3=1 to I_3
  Calculating the L based on (10)
  for i=1 to N
    Update the w_{t+1} with (13)
  end for
end for

/* Operation Ending */

Output: w_{t+1}

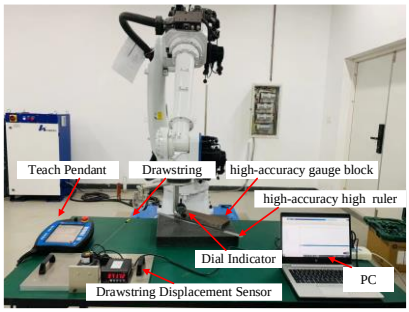

Fig. 1. Experimental system.

$$
\begin{aligned}
L &= \arg\min_{w} \left\| Y_i - F_i(\hat{w}) \right\|_2^2 \\
&= \frac{1}{2N}\sum_{i=1}^{N} \left\| Y_i - F_i(\hat{w}_t, P_{0,t}) - \nabla_{\hat{w}_t} F_i(\hat{w}_{t+1} - \hat{w}_t) - \nabla_{P_{0,t}} F_i(P_{0,t+1} - P_{0,t}) \right\|_2^2 \\
&\quad + \frac{1}{2N}\sum_{r}^{K,M} \rho_r \sum_{i=1}^{N} \left\| \Phi_{i,r}(\hat{w}_t, \hat{P}_t, \beta'_t) + \nabla_{\hat{w}_t} \Phi_{i,r}(\hat{w}_{t+1} - \hat{w}_t) \right. \\
&\quad \left. + \nabla_{P_t} \Phi_{i,r}(\hat{P}_{t+1} - \hat{P}_t) + \nabla_{\beta_t} \Phi_{i,r}(\beta'_{t+1} - \beta'_t) \right\|_2^2 \\
&\quad + \frac{\lambda}{2}\left[(\hat{w}_{t+1} - \hat{w}_t)^2 + (P_{0,t+1} - P_{0,t})^2 + (\hat{P}_{t+1} - \hat{P}_t)^2 + (\beta'_{t+1} - \beta'_t)^2 \right], \\
s.t. &\forall r \in \{K, M\},
\end{aligned}
\tag{10}
$$

where ρ is the constraint coefficient of the spatial line. Hence, we update the w_t, β_t and P_t as:

$$
\begin{aligned}
\beta'_{t+1} &= \beta'_t + \left[\frac{1}{N}\sum_{i=1}^{N}\sum_{r}^{K,M} \left(\rho_r \frac{\partial \Phi_{r,i}}{\partial \beta'_t} \left(\frac{\partial \Phi_{r,i}}{\partial \beta'_t} \right)^T \right) + \lambda I_0 \right]^{-1} \\
&\quad \times \frac{1}{N}\sum_{i=1}^{N}\sum_{r}^{K,M} \left(\rho_r \Phi_{r,i} \frac{\partial \Phi_{r,i}}{\partial \beta'_t} \right),
\end{aligned}
\tag{11}
$$

TABLE II. THE COMPARED ALGORITHM S.

No.	Description
M1	PSO (Particle swarm optimization) with a spatial line constraint. The PSO algorithm simulates the predation behavior of bird flocks [14].
M2	EKF (extended Kalman filter) with a spatial line constraint. The EKF algorithm can be addressed the issue of non-Gauss noise [3].
M3	UKF (Unscented Kalman filter) with a spatial line constraint. The UKF algorithm is introduced in [25].
M4	LS (Least squares) with a spatial line constraint. The LS algorithm is introduced in [1], [31].
M5	SA (simulate anneal) with a spatial line constraint in [14]
M6	PF (Particle filter) with a spatial line constraint. The PF can decrease noises as mentioned in [3].
M7	Differential Evolution (DE) with a spatial line constraint in [28].
M8	LMLC algorithm is introduced in Section III(B).
M9	The MCS-LMLC calibrator.

TABLE III. Calibration Accuracy.

No.	RMSE(mm)	MEAN(mm)	MAX(mm)
Before	2.58	2.49	4.50
M1	0.72	0.65	1.53
M2	0.91	0.81	1.81
M3	0.87	0.78	1.73
M4	0.62	0.53	1.27
M5	0.76	0.65	1.46
M6	0.81	0.70	1.61
M7	0.66	0.56	1.38
M8	0.60	0.51	1.10
M9	0.56	0.46	0.91

TABLE IV. TIME COST OF ALL COMPARED ALGORITHMS.

No.	Total Time Cost(s) (RMSE)	Average Iteration Count (RMSE)
M1	52.53	50
M2	16	12
M3	22.3	20
M4	65.19	70
M5	66.96	65
M6	18.2	16
M7	61.56	56
M8	36.32	10
M9	32.31	2

TABLE V. INDUSTRIAL ROBOT KINEMATIC PARAMETERS AFTER CALIBRATION.

Joint i	α_i (°)	a_i (mm)	d_i (mm)	θ_i (°)
1	-89.9821	250.9333	653.2808	0.5689
2	-0.0351	895.6871	-0.2853	-90.9003
3	90.0153	-206.9612	-0.1999	180.0695
4	-90.1516	0.1586	1033.9127	0.5098
5	90.1056	-0.2399	0.3612	90.3276
6	0.1102	-0.2560	199.7680	0.9653

$$
\begin{aligned}
\hat{P}_{t+1} &= \hat{P}_t + \left[\frac{1}{N}\sum_{i=1}^{N}\sum_{r}^{K,M} \left(\rho_r \frac{\partial \Phi_{r,i}}{\partial \hat{P}_t} \left(\frac{\partial \Phi_{r,i}}{\partial \hat{P}_t} \right)^T \right) + \lambda I_0 \right]^{-1} \\
&\quad \times \frac{1}{N}\sum_{i=1}^{N}\sum_{r}^{K,M} \left(\rho_r \Phi_{r,i} \frac{\partial \Phi_{r,i}}{\partial \hat{P}_t} \right),
\end{aligned}
\tag{12}
$$

$$
\begin{aligned}
\hat{w}_{t+1} &= \hat{w}_t + \frac{1}{N}\left[\sum_{i=1}^{N} \left(\frac{\partial F_i}{\partial \hat{w}_t} \left(\frac{\partial F_i}{\partial \hat{w}_t} \right)^T + \sum_{r}^{K,M} \rho_r \frac{\partial \Phi_{r,i}}{\partial \hat{w}_t} \left(\frac{\partial \Phi_{r,i}}{\partial \hat{w}_t} \right)^T \right) + \lambda I_0 \right]^{-1} \\
&\quad \times \frac{1}{N}\sum_{i=1}^{N} \left[\frac{\partial F_i}{\partial \hat{w}_i} (Y_i - F_i) + \sum_{r}^{K,M} \rho_r \Phi_{r,i} \left(\frac{\partial \Phi_{r,i}}{\partial \hat{w}_t} \right)^T \right],
\end{aligned}
\tag{13}
$$

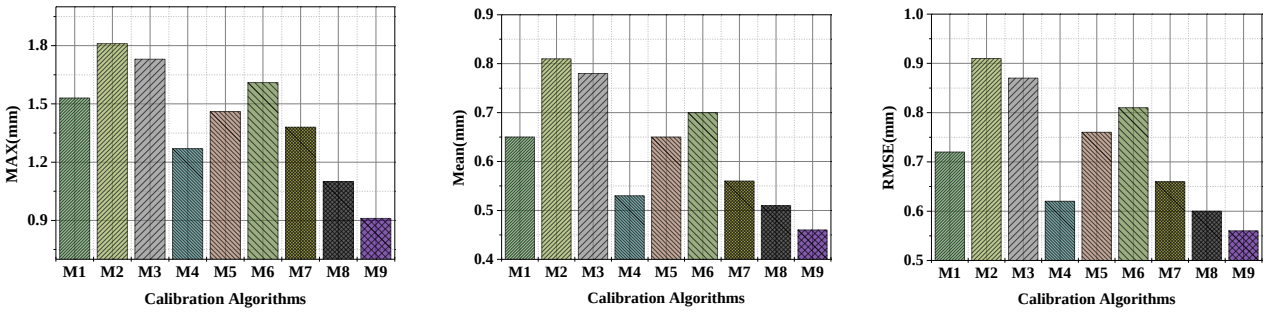

(a) (b) (c)

Fig. 2. The calibration accuracy. (a) RMSE of compared calibrators. (b) MEAN of compared calibrators. (c) MAX of compared calibrators.

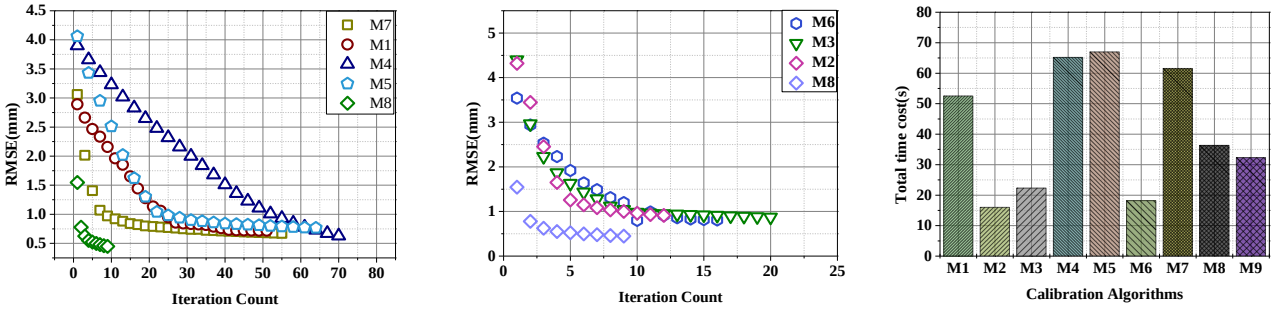

(a) (b) (c)

Fig. 3. The training curves and time cost of all calibrators. (a) Training curves of M7, M1, M4, M5, M8. (b) Training curves of M6, M3, M2, M8. (c) Time costs of M1-9.

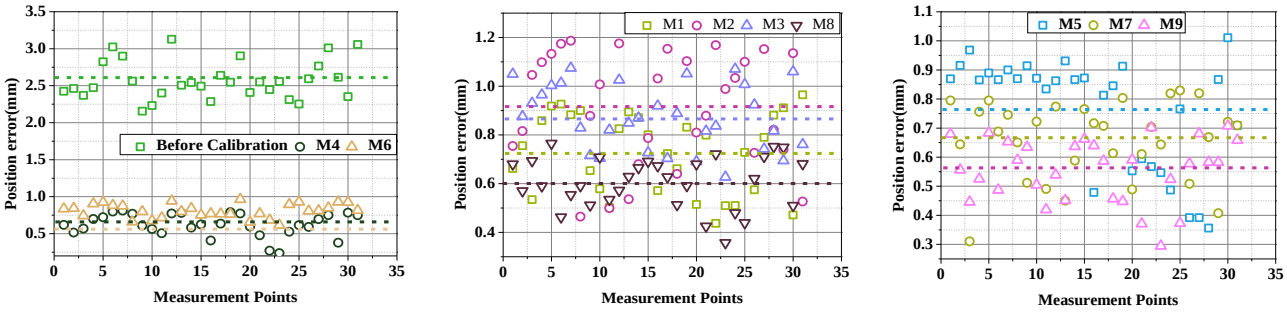

(a) (b) (c)

Fig. 4. The industrial robot's positioning errors after calibration by M1-9. (a)Position errors before calibration, M4 and M6. (b)Position errors of M1, M2, M3 and M8. (c)Position errors of M5, M7 and M9. The results illustrate that M9 has the best robot calibration accuracy.

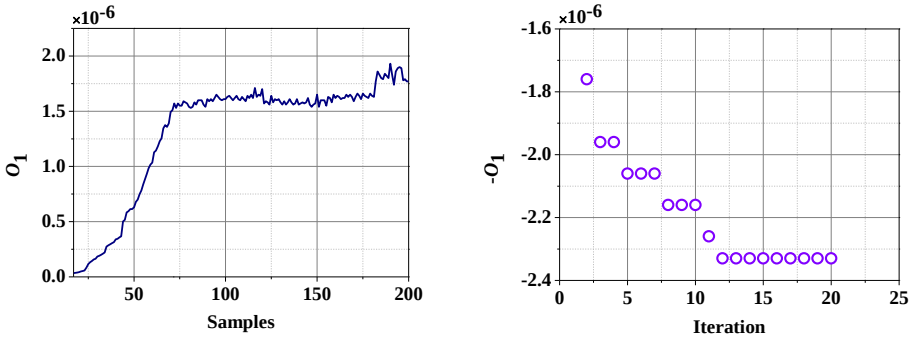

Fig. 5. The MCS's results. (a)The effects of measurement configurations' number. (b)The process of the optimal measurement configurations selection.

Algorithm I: Procedure MCS-LMLC calibrator, which can effectively calibrate the kinematic parameters. In this calibrator, I_1 refers to the max iteration round for the SA algorithm, I_2 and I_3 are the max iteration round for the LMLC algorithm for updating β'_{t+1}, $\hat{P}_{t+1}$ and $\hat{w}_{t+1}$, $\{q_{i,1}, q_{i,2}, \ldots, q_{i,6}\}$ are the torsion angles of a robot. p_0, P_0 and β_0 are the initial coordinates of the fixed point on the ground, the initial point on the spatial line and the initial direction vector of a spatial line.

III. EXPERIMENTAL RESULTS

This section mainly carries out enough experiments on an HRS JR680 industrial robot for verifying the performance of the MCS-LMLC calibrator.

A. Experimental Setup

Fig. 1 shows an experimental system, which includes a drawstring displacement indicator, a drawstring displacement sensor, an HSR-JR680 industrial robot, a dial indicator, a PC, a high-accuracy ruler and a high-accuracy gauge block.

B. Evaluation Metrics

This work adopts maximum error (MAX), mean error (MEAN) and root mean squared error (RMSE) as the evaluation metrics [28]-[34]:

$$MAX = max\left(\sqrt{\left(Y_i - F\left(w\right)\right)^2}\right), i = 1, 2, ..., N$$

$$MEAN = \frac{1}{N}\sum_{i=1}^{N}\left(\sqrt{\left(Y_i - F\left(w\right)\right)^2}\right),$$

$$RMSE = \sum_{i=1}^{N}\left(\sqrt{\frac{1}{N}\left(Y_i - F\left(w\right)\right)^2}\right).$$

C. Experimental Process

In the experimental process, we first collect 200 samples on a spatial line of the high-accuracy gauge block, each of which includes six torsion angles, the length of the drawstring, and a reading of the dial indicator. The optimal measurement samples are selected by the MCS method. Then we adopt the proposed algorithm for kinematic parameter identification. Finally, we can achieve improvement in the robot's accuracy by compensating for the errors. The calibrators are listed in Table II.

D. Compared Systems

To verify the MCS-LMLC calibrator's performance, we carefully compare it to several state-of-the-art calibrators. The calibration accuracies are depicted in Table III. The time costs of all calibrators are illustrated in Table IV. Moreover, Fig. 2-4 show M1-9's calibration accuracies, the training curves, and the positional errors. Based on the above results, we can summarize the following findings:

a) The LMLC algorithm significantly outperforms its peers in terms of the calibration accuracy of a robot. Compared with M1-7's calibration accuracy, M8 is the highest. From Fig. 2 and Table III, M8's RMSE, MEAN and MAX are 0.60mm, 0.51mm and 1.10mm, respectively, which are about 16.67%, 21.53% and 28.10% lower than M1's 0.72mm, 0.65mm and 1.53mm, 34.06%, 37.03% and 39.22% lower than M2's 0.91mm, 0.81mm and 1.81mm, 31.03%, 34.62% and 36.42% lower than M3's 0.87mm, 0.78mm and 1.73mm, 3.22%, 3.77% and 13.39% lower than M4's 0.62mm, 0.53mm and 1.27mm, 21.05%, 21.53% and 24.66% lower than M5's 0.76mm, 0.65mm and 1.46mm, 25.93%, 27.14% and 31.68% lower than M6's 0.81mm, 0.70mm and 1.61mm, 9.09%, 8.93% and 20.29% lower than M3's 0.66mm, 0.56mm and 1.38mm. Hence, the LMLC algorithm's calibration accuracy significantly outperforms the proposed state-of-the-art calibrators.

b) **The MCS method can effectively decrease measurement noises for enhancing the stability of experimental results.** We take the O_1 as an example. As depicted in Fig. 5(a), with the enhancement of the number of measurement configurations, the O_1 is flat at about 72 configurations. Then, according to the results of it, we employ the SA algorithm to achieve the optimal measurement configurations selection, as shown in Fig. 5(b). Subsequently, we identify the kinematic parameters based on the optimal measurement configurations. As listed in Table III and depicted in Fig. 2, M9's RMSE, Mean and MAX are 7.12%, 10.87% and 20.88% lower than M8's 0.56mm, 0.46mm and 0.91mm. Thus, MCS is beneficial to enhance robot calibration accuracy.

c) MCS-LMLC calibrator has a competitive computational efficiency. As illustrated in Fig. 3(a)-(b) and Table IV, M8's convergence rate is fast, which involves 10 iterations compared with M1-7. Thus, the LMLC algorithm converges fast. Moreover, M9 takes 32.31s to converge, which is higher than M2-3 and M6. However, it is 38.49% lower than M1's 52.53s, 50.48% lower than M4's 65.19s, 51.75% lower than M5's 66.96s, 47.51% 47.51% lower than M7's 61.56s, 11.04% lower than M4's 36.32s. Thus, the proposed calibrator has a competitive computational efficiency.

d) MCS-LMLC calibrator can significantly diminish the position errors of the industrial robot. Table V records the D-H parameters after calibration. Moreover, 30 configurations from 72 configurations are randomly selected to compare M1-9's performance, as depicted in Fig. 4. The results illustrate that the position errors of the industrial robot are significantly diminished, and M9 is minimal compared with M1-8. Hence, the proposed MCS-LMLC calibrator is practically feasible with a high robot calibration accuracy and without overfitting risk.

A. Summary

According to the above analysis, we summarize the following deductions for robot calibration of the MCS-LMPC calibrator.

a) It has an excellent calibration accuracy on an HSR-JR680 industrial robot,

b) It can effectively enhance the stability of experimental results.

c) It converges fast, and

d) It achieves a competitive computational efficiency.

IV. Conclusions

To accurately calibrate an industrial robot, we propose an MCS-LMLC calibrator. The MCS method is adopted to decrease measurement noises to enhance the stability of experimental results. LMLC algorithm is presented to address the issue of kinematic parameter identification. Enough experiments strongly support a competitive robot calibration performance for the proposed MCS-LMLC calibrator. Hence, a highly feasible robot calibrator is developed for industrial robot applications. To date, the following issues remain open:

a) Acceleration methods like GPU deserve to be studied in improving the compatibility of the MCS-LMLC calibrator.

b) Reducing the dynamic errors of an industrial robot is highly interesting.

c) To achieve online calibration is also desired.

V. Acknowledgment

This research is supported in part by the National Natural Science Foundation of China under grants 62002337, and in part by the CAAI-Huawei MindSpore Open Fund under grants CAAIXSJLJJ-2021-035A.

References

[1] G. Y. Luo, L. Zou, Z. L. Wang, C. Lv, J. Ou, and Y. Huang, “A novel kinematic parameters calibration method for industrial robot based on Levenberg-Marquardt and Differential Evolution hybrid algorithm,” *Robotics and Computer-Integrated Manufacturing*, vol. 71, pp. 102165, Oct, 2021.

[2] X. Luo, Y. Zhou, Z. Liu, and M. Zhou, “Fast and accurate non-negative latent factor analysis on high-dimensional and sparse matrices in recommender systems,” *IEEE Transactions on Knowledge and Data Engineering*, vol. 35, no. 4, pp. 3897-3911, Apr. 2023.

[3] Z. Jiang, W. Zhou, H. Li, Y. Mo, W. Ni, and Q. Huang, “A new kind of accurate calibration method for robotic kinematic parameters based on the extended Kalman and particle filter algorithm,” *IEEE Transactions on Industrial Electronics*, vol. 65, no. 4, pp. 3337–3345, Apr. 2018.

[4] X. Luo, H. Wu, and Z. Li, “NeuLFT: A novel approach to nonlinear canonical polyadic decomposition on high-dimensional incomplete tensors,” *IEEE Transactions on Knowledge and Data Engineering*, vol. 35, no. 6, pp. 6148-6166, Jun. 2023.

[5] S. Li, Y. Zhang and L. Jin, “Kinematic Control of Redundant Manipulators Using Neural Networks,” *IEEE Transactions on Neural Networks and Learning Systems*, vol. 28, no. 10, pp. 2243-2254, Oct. 2017.

[6] T. S. Lembono, F. Suárez-Ruiz, and Q. C. Pham, “SCALAR: Simultaneous calibration of 2-D laser and robot kinematic parameters using planarity and distance constraints,” *IEEE Trans. Autom. Sci. Eng.*, vol. 16, no. 4, pp. 1971-1979, Oct. 2019.

[7] X. Luo, D. Wang, M. Zhou and H. Yuan, "Latent factor-based recommenders relying on extended stochastic gradient descent algorithms," *IEEE Transactions on Systems, Man, and Cybernetics: Systems*, vol. 51, no. 2, pp. 916-926, Feb. 2021.

[8] D. Wu, X. Luo, M. Shang, Y. He, G. Wang and M. Zhou, “A deep latent factor model for high-dimensional and sparse matrices in recommender systems,” *IEEE Transactions on Systems, Man, and Cybernetics: Systems*, vol. 51, no. 7, pp. 4285-4296, Jul. 2021.

[9] C. T. Mao, S. Li, Z. W. Chen, X. Zhang, and C. Li, “Robust kinematic calibration for improving collaboration accuracy of dual-arm manipulators with experimental validation,” *Measurement*, vol. 155, pp. 107524, Apr. 2020.

[10] X. Luo, M. Zhou, S. Li, D. Wu, Z. Liu and M. Shang, “Algorithms of unconstrained non-negative latent factor analysis for recommender systems,” *IEEE Transactions on Big Data*, vol. 7, no. 1, pp. 227-240, March 2021.

[11] S. Li, J. He, Y. Li and M. U. Rafique, “Distributed Recurrent Neural Networks for Cooperative Control of Manipulators: A Game-Theoretic Perspective,” *IEEE Transactions on Neural Networks and Learning Systems*, vol. 28, no. 2, pp. 415-426, Feb. 2017.

[12] X. Luo, M. Zhou, S. Li, L. Hu and M. Shang, "Non-Negativity constrained missing data estimation for high-dimensional and sparse matrices from industrial applications," *IEEE Transactions on Cybernetics*, vol. 50, no. 5, pp. 1844-1855, May 2020.

[13] Z. Jiang, M. Huang, X. Tang and Y. Guo, “A new calibration method for joint-dependent geometric errors of industrial robot based on multiple identification spaces,” *Robotics and Computer-Integrated Manufacturing*, vol. 71, p. 102175, Oct. 2021.

[14] W. Wang, H. Song, Z. Yan, L. Sun, Z. Du, “A universal index and an improved PSO algorithm for optimal pose selection in kinematic calibration of a novel surgical robot,” *Robotics and Computer-Integrated Manufacturing*, vol. 50, pp. 90-101, Apr. 2018.

[15] X. Luo, H. Wu, H. Yuan and M. Zhou, "Temporal pattern-aware qos prediction via biased non-negative latent factorization of tensors," *IEEE Transactions on Cybernetics*, vol. 50, no. 5, pp. 1798-1809, May 2020.

[16] W. Li, X. Luo, H. Yuan, and M. Zhou, "A momentum-accelerated hessian-vector-based latent factor analysis model," *IEEE Transactions on Services Computing*, vol. 16, no. 2, pp. 830-844, March-April 2023.

[17] Z. X. Jiang, M. Huang, X. Q. Tang, B. Song, and Y. X. Guo, “Observability index optimization of robot calibration based on multiple identification spaces,” *Autonomous Robots*, vol. 44, no. 8, pp. 1029–1046, 2020.

[18] Z. Fu, J. S. Dai, K. Yang, X. Chen, and P. López-Custodio, “Analysis of unified error model and simulated parameters calibration for robotic machining based on Lie theory,” *Robotics and Computer-Integrated Manufacturing*, vol. 65, pp. 101855, Feb. 2020.

[19] W. Li, Q. He, X. Luo and Z. Wang, "Assimilating second-order information for building non-negative latent factor analysis-based recommenders," *IEEE Transactions on Systems, Man, and Cybernetics: Systems*, vol. 52, no. 1, pp. 485-497, Jan. 2022.

[20] D. Wu, and X. Luo, "Robust latent factor analysis for precise representation of high-dimensional and sparse data," *IEEE/CAA Journal of Automatica Sinica*, vol. 8, no. 4, pp. 796-805, Apr. 2021.

[21] C. Mao, Z. Chen, S. Li, X. Zhang, “Separable nonlinear least squares algorithm for robust kinematic calibration of serial robots,” *Journal of Intelligent & Robotic Systems*, vol. 101, no. 1, Jan. 2021.

[22] Z. Li, S. Li and X. Luo, "Efficient industrial robot calibration via a novel unscented Kalman filter-incorporated variable step-size Levenberg-Marquardt algorithm," *IEEE Transactions on Instrumentation and Measurement*, doi: 10.1109/TIM.2023.3265744.

[23] X. Luo, Z. Liu, S. Li, M. Shang and Z. Wang, "A fast non-negative latent factor model based on generalized momentum method," *IEEE Transactions on Systems, Man, and Cybernetics: Systems*, vol. 51, no. 1, pp. 610-620, Jan. 2021.

[24] X. Deng, L. Ge, R. Li and Z. Liu, “Research on the kinematic parameter calibration method of industrial robot based on LM and PF algorithm,” in *Proc. of the 32th Int. Conf. on Chinese Control and Decision*, Hefei, China, Aug. 2020, pp. 2198-2203.

[25] G. Du, Y. Liang, C. Li, P. X. Liu and D. Li, “Online robot kinematic calibration using hybrid filter with multiple sensors,” *IEEE Transactions on Instrumentation and Measurement*, vol. 69, pp. 7092-7107, Sept. 2020.

[26] Z. Li, S. Li, A. Francis and X. Luo, "A Novel Calibration System for Robot Arm via an Open Dataset and a Learning Perspective," *IEEE Transactions on Circuits and Systems II: Express Briefs*, vol. 69, no. 12, pp. 5169-5173, Dec. 2022.

[27] X. Luo, M. Shang and S. Li, "Efficient extraction of non-negative latent factors from high-dimensional and sparse matrices in industrial applications," *2016 IEEE 16th International Conference on Data Mining (ICDM)*, Barcelona, Spain, 2016, pp. 311-319.

[28] J. W. Yan, B. Pan, Y. L. Fu, “Ultrasound-guided prostate percutaneous intervention robot system and calibration by informative particle swarm optimization,” *Frontiers of Mechanical Engineering*, vol. 17, no. 1, pp. 1-16, Mar. 2022.

[29] W. Yang, S. Li, Z. Li and X. Luo, "Highly-Accurate Manipulator Calibration via Extended Kalman Filter-Incorporated Residual Neural Network," *IEEE Transactions on Industrial Informatics*, doi: 10.1109/TII.2023.3241614.

[30] D. Wu, Y. He, X. Luo and M. Zhou, "A latent factor analysis-based approach to online sparse streaming feature selection," *IEEE Transactions on Systems, Man, and Cybernetics: Systems*, vol. 52, no. 11, pp. 6744-6758, Nov. 2022.

[31] Z. Li, S. Li, O. O. Bamasag, A. Alhothali and X. Luo, “Diversified regularization enhanced training for effective manipulator calibration,” *IEEE Transactions Neural Networks and Learning Systems*, DOI: 10.1109/TNNLS.2022.3153039.

[32] Z. B. Li, S. Li, and X. Luo, “An overview of calibration technology of industrial robots,” *IEEE/CAA Journal of Automatica Sinica*, vol. 8, no. 8, 23-36, Jan. 2021.

[33] K. Kamali, and I. A. Bonev, “Optimal experiment design for elasto-geometrical calibration of industrial robots,” *IEEE/ASME Transactions on Mechatronics*, vol. 24, no. 6, pp. 2733-2744, Dec. 2019.

[34] T. Chen, S. Li, and H. Wu, "Highly-Accurate robot calibration based on plane constraint via integrating Square-Root Cubature Kalman filter and Levenberg-Marquardt algorithm," *2022 IEEE International Conference on Networking, Sensing and Control (ICNSC)*, Shanghai, China, pp. 1-6, 2022.